SINTEF

This is the Accepted version of the article

Performance and reliability of PZT-based piezoelectric micromirrors operated in realistic environments

R. P. Dahl-Hansen, T. Tybell, F. Tyholdt

Citation:
R. P. Dahl-Hansen, T. Tybell, F. Tyholdt (2018) Performance and reliability of PZT-based piezoelectric micromirrors operated in realistic environments. In: 2018 IEEE ISAF-FMA-AMF-AMEC-PFM Joint Conference (IFAAP), Hiroshima, Japan, 27 May-1 June 2018
DOI: 10.1109/ISAF.2018.8463243

This is the Accepted version.
It may contain differences form the journal's pdf version

This file was downloaded from SINTEFs Open Archive, the institutional repository at SINTEF
http://brage.bibsys.no/sintef

Performance and reliability of PZT-based piezoelectric micromirrors operated in realistic environments

R. P. Dahl-Hansen[1,2*], T. Tybell[1]
[1]Norwegian University of Science and Technology
Department of Electronic Systems,
7491, Trondheim, Norway

F. Tyholdt[2]
[2]SINTEF Digital, MiNaLab,
Gaustadalleen 23C, 0373, Oslo, Norway
*runarplu@ntnu.no

***Abstract*—The number of application areas for piezoelectric microelectromechanical systems based on PZT have increased rapidly over the years. Thus, to continue the development towards commercial deployment, characterizing lifetime and reliability during operation in realistic and harsh environments is important. Such environments are demanding for piezoMEMS devices since they often involve high humidity levels and elevated temperatures which gives rise to complex degradation. To address how such conditions affects device performance we combined optical and electrical measurements to elucidate the degradation of a PZT-based thin-film piezoelectric MEMS micromirror during temperature-humidity-cycling tests. As a test structure, $1\ \mu m$ $PbZr_{0.40}Ti_{0.60}O_3$ on a $10\ nm$ $LaNiO_3$ buffer-layer, were deposited by pulsed laser deposition on platinized Silicon-on-Insulator wafers. A 250 nm Au/TiW top electrode was deposited by DC-sputtering before structuring the final device. The micromirrors were unipolarly actuated with a signal of $20\ V$ peak-to-peak at a frequency of $1.5\ kHz$ in an ambient with constant vapor concentration of $22\ g/m^3$ for device temperatures between $25\ ^oC$ and $175\ ^oC$. Humidity-related degradation was manifested as local breakdown events and pinholes on top of and along the edges of the used electrodes. This had a strong effect on device performance and preceded degradation due to polarization-fatigue at all temperatures. Also, both the initial piezoelectric response and number of cycles to device failure increased with increasing substrate temperature in humid ambient.**

Keywords: PiezoMEMS reliability, lifetime, fatigue, temperature, humidity

I. Introduction

Due to its large piezoelectric response, $PbZr_xTi_{1-x}O_3$ (PZT) is commonly used for piezoelectric microelectromechanical systems (piezoMEMS) including RF-switches, ultrasonic transducers, gas sensors and micromirrors [1], [2]. Prior to commercialization, cycling tests in humid ambient and at elevated temperatures are important to assess the reliability of piezoMEMS-devices operated in realistic and harsh environments. Device operation in high humidity are associated with the early onset of irreversible degradation, including elemental migration, cracking and local breakdown events [3]. This primarily occurs in close vicinity to the used electrodes and originates from electrical, mechanical and electrochemical processes occurring both within PZT and on the PZT and electrode surfaces during operation. Elevated temperatures on the other hand will impact the reversible degradation mechanisms due to changes in the dielectric and piezoelectric properties, as well as increase the leakage and change the stress-strain relations of the structure [4]–[6]. Since thin-film piezoMEMS-devices in general rely heavily on the stress-transfer between the film and substrate, in-plane changes caused by any such degradation may have major implications on the electromechanical response and therefore the device performance. Hence it is important to assess how the piezoelectric response, lifetime and reliability of each piezoMEMS-device is affected by elevated temperature and ambient humidity.

In the current work we investigated the degradation and electromechanical response of bimorph PZT-based thin film micromirrors during operation in humid ambient and elevated temperatures.

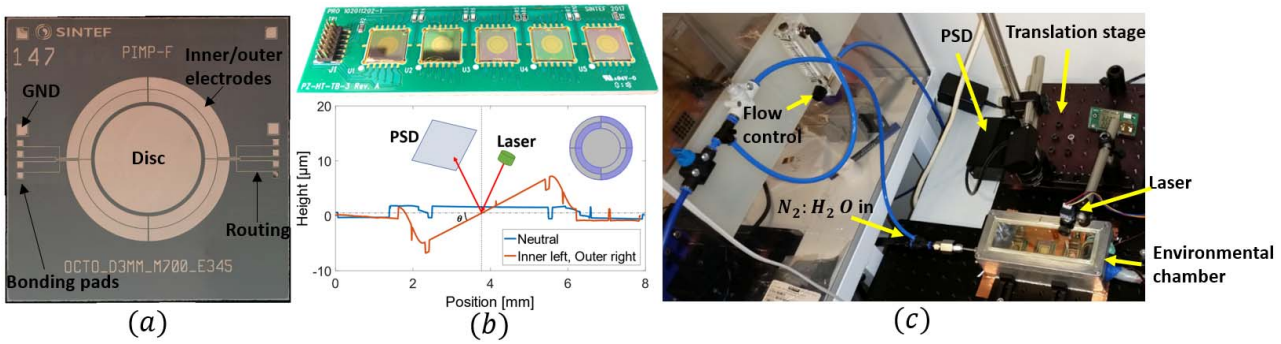

(a) (b) (c)

Figure 1: Device and experimental setup. (a): structure of the tested micromirror, (b): MEMS test-circuit for simultaneous testing of five micromirrors and actuation giving the maximum 2D tilt of $\pm 0.5^o$ The laser was reflected of the mirror onto a position sensitive device (PSD). (c): environmental chamber and experimental setup. The ambient was kept constant with an absolute humidity of 22 g/m^2 and the micromirrors were heated from below by a hot-plate.

978-1-5386-1162-3/18/$31.00 ©2018 IEEE

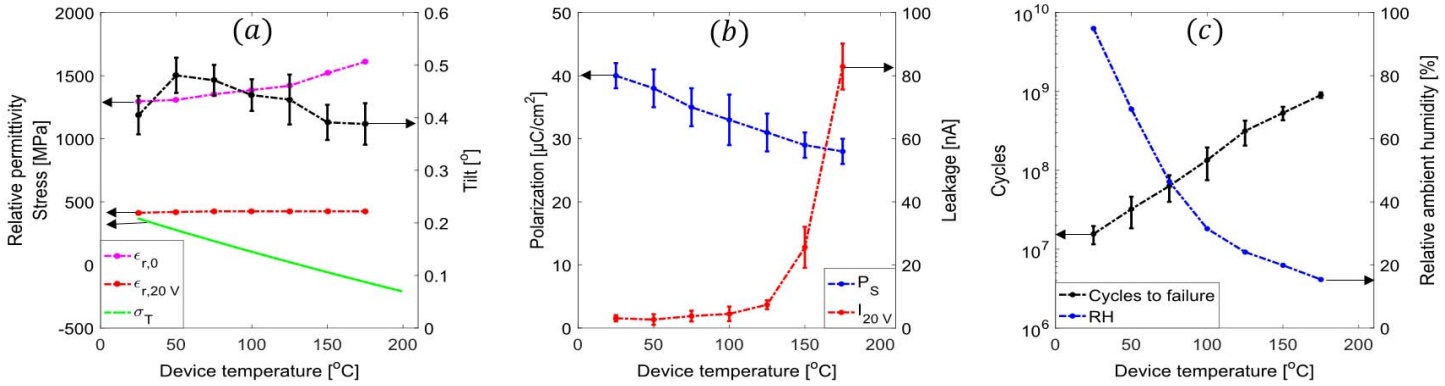

Figure 2: (a): Measured relative permittivity at 0 V, $\varepsilon_{r,0}$, and 20 V, $\varepsilon_{r,20\,V}$, calculated thermal stress, σ_T, and deflection tilt as a function of device temperature. (b): average polarization and leakage as a function of device temperature. (c): Average cycles to failure, and relative humidity due to heated ambient as a function of device temperature.

II. Methods

Piezoelectric micromirrors, see *Fig. 1* (a), were fabricated according to literature [1] using 1 µm pulsed laser-deposited Ba-doped $PbZr_{0.40}Ti_{0.60}O_3$. The mirror consisted of a rigid Silicon disc $3\,mm$ in diameter, suspended on a flexible membrane surrounded by eight integrated PZT-actuators. 2D tilt and out-of-plane movement was enabled by actuating the inner and outer electrodes according to *Fig. 1* (b). For the micromirrors used in this work, a maximum 2D tilt of $\pm 0.5^o$ was achieved by simultaneously actuating the two inner and two outer electrodes on opposite sides of the center disc. Five micromirrors were wire-bonded to a test-circuit and actuated in parallel inside the environmental chamber for each test condition. The ambient vapor concentration was kept constant at $22\ g/m^3$ by bubbling N_2 through a DI-water container and introducing the mixture into the chamber as shown in *Fig. 1* (c). Humidity and ambient temperature (T_{atm}) was measured using a HYT271 humidity-sensor and the micromirrors heated from below by a hotplate. The micromirror temperature (T_{sub}) was measured using a k-type thermocouple attached to the surface of one of the tested devices.

After ambient stabilization, the micromirrors were unipolarly actuated with a peak-to-peak voltage (V_{PP}) of $20\ V$ at $1.5\ kHz$ while T_{sub} was varied in steps of $25\ ^oC$ from $25\ ^oC$ to $175\ ^oC$. A laser was reflected of the micromirror through an optical window onto a position sensitive device (PSD) for electromechanical characterization. The recorded x -and y-positions of the laser trace were then used to approximate the deflection tilt according to:

$$tan(2\theta) \approx 2\theta = \frac{\sqrt{x^2 + y^2}}{l}\ [rad] \qquad (1)$$

where θ is the achieved angular deflection of the micromirror according to the neutral plane, see *Fig. 1* (b), and l the length from the device to the PSD. Ferroelectric characterization was done by retrofitting an aixACCT TF2000 Analyzer to the experimental setup. Ferroelectric hysteresis was measured at $10\ Hz$ with a large-signal of $-25\ V$ to $25\ V$, the capacitance-measurements with a small-signal amplitude of $200\ mV$ at $1\ kHz$ and the leakage with steps of $2\ V$ and $2\ sec$ dwell from $-20\ to\ 20\ V$.

III. Results and Discussion

A. Electromechanical response

Fig. 2 (a) show the measured average angular tilt, relative permittivity at 0 V ($\varepsilon_{r,0\,V}$) and 20 V ($\varepsilon_{r,20\,V}$) and calculated total thermal stress in the device stack (σ_T) plotted as a function of T_{sub}. The measured average saturation polarization (P_S) and leakage at $20\ V$ ($I_{20,V}$) is shown in *Fig. 2* (b) and the values summarized in *Table I*. $\varepsilon_{r,0}$, $\varepsilon_{r,20\,V}$ and $I_{20\,V}$ increases, while P_S decreases with increasing T_{sub} and is consistent with literature on ferroelectrics [5]. As shown in *Fig. 2* (a) the measured average tilt increases with T_{sub} and peaks at 50^oC before it decreases for $T_{sub} > 50\ ^oC$. Such electromechanical behavior has also been reported for similar PZT-based ceramics in literature [7]. Thin-film devices such as the present micromirror, are particularly sensitive to the in-plane circumstances. Hence in-plane stress, excitation field and device geometry are important for the final electromechanical response. The bending moment moving the current device structure originates from the total in-plane stress (σ_{tot}) and has three main contributions: the residual stress (σ_R) applied stress (σ_A) and piezoelectric stress (σ_P). The latter being the controllable stress, relates to the

Table I: Average measured values

Device	T_{sub} [^oC]	T_{atm} [^oC]	**Tilt** [deg]	**Cycles to failure**	$\varepsilon_{r,0}$	$\varepsilon_{r,20}$	P_R [$\frac{\mu C}{cm^2}$]	P_S [$\frac{\mu C}{cm^2}$]	I^+ [nA]	σ_T [MPa]	**RH** [%]
1 – 5	25	25.0	0.40 ± 0.04	$1.6x10^7 \pm 0.4x10^7$	1297	414	10.3	40 ± 2	3.1 ± 1.0	*368*	95.0
6 – 10	50	30.8	0.48 ± 0.03	$3.2x10^7 \pm 1.4x10^7$	1308	420	10.3	38 ± 3	2.7 ± 1.7	*284*	69.4
11 – 15	75	38.5	0.47 ± 0.03	$6.3x10^7 \pm 2.3x10^7$	1353	424	9.3	35 ± 3	3.8 ± 1.7	*196*	46.4
16 – 20	100	46.4	0.44 ± 0.03	$13.5x10^7 \pm 6.0x10^7$	1387	425	8.3	33 ± 4	4.5 ± 2.3	*111*	31.5
21 – 25	125	52.1	0.43 ± 0.04	$31.6x10^7 \pm 10.9x10^7$	1420	425	7.9	31 ± 3	7.4 ± 1.4	*29*	24.1
26 – 30	150	56.4	0.40 ± 0.03	$53.5x10^7 \pm 10.4x10^7$	1521	425	8.0	29 ± 2	25.6 ± 6.5	*-51*	19.9
31 – 35	175	62.3	0.39 ± 0.04	$90.0x10^7 \pm 7.2x10^7$	1610	425	8.0	28 ± 2	82.9 ± 7.3	*-129*	15.4

TABLE II: VALUES FOR THERMAL STRESS CALCULATION

Material	$E\ [GPa]$	ν	$\alpha x10^{-6}\ [K^{-1}]$	$T_{dep}\ [^oC]$	*Ref.*
Au	*78*	*0.44*	*14.2*	*25*	*[5]*
PZT	*161*	*0.31*	*6*	*620*	*[5]*
Pt	*168*	*0.38*	*9*	*450*	*[5]*
SiO_2	*70*	*0.3*	*0.6*	1050	*[5]*
Si	*170*	*0.28*	$\alpha = -15.2459 + 3.43026lnT$	*N/A*	*[8]*

transverse electric field, E_z, and the effective in-plane piezocoefficient, $e_{31,f}$ by $\sigma_P = -e_{31,f}E_z$. $e_{31,f}$ is proportional to P_S and ε_r measured out-of-plane (along the 3-direction), i.e. $e_{31,f} \propto -2\varepsilon_{33}P_3$ [5]. Since the relative decrease in P_S seems to be larger than the relative increase in $\varepsilon_{r,0}$ and $\varepsilon_{r,20}$, the net σ_P (and total deflection) is expected to decrease with increasing temperature. From the measured values of P_S and ε_r, this should correspond to a net decrease of the total in-plane stress by 4.2 % at 50^oC. On the contrary, the measured initial deflection is indeed increasing by 20 % from 25 ^oC to 50 ^oC, and remains larger than the room-temperature deflection up to $T_{sub} = 175\ ^oC$. We suggest that this is partly due to stress changes in the stack where $\sigma_{tot} = \sigma_R + \sigma_A + \sigma_P$. A large portion of the residual stress is the thermal stress between the film and substrate given by:

$$\sigma_T = \frac{E_{film}\left(\alpha_{film} - \alpha_{sub}\right)\Delta T}{\left(1 - \nu_{film}\right)}\ [MPa] \qquad (2)$$

where α is the thermal expansion coefficients of the used materials, E_{film} is the Young's modulus, ν_{film} is the Poisson ratio and ΔT is the difference between the deposition and T_{sub}. Here a positive sign corresponds to a tensile stress and a negative sign to a compressive stress. As a simple first order approximation, σ_T was calculated for the adjacent films and added together for the entire stack (for exact stress-calculations of multi-layered stacks, the thickness and device geometry must also be considered). The linear thermal expansion coefficient was used for all materials except Si which displays the largest nonlinearities in the relevant temperature range [8]. *TABLE II* summarizes the used thermal expansion values and the calculated σ_T at the different T_{sub} can be found in *Fig. 2* (a) and *TABLE I*. Despite the simplicity of the used model the calculated stresses correlate well with measured values from previous wafer bending experiments.

PLD-deposited PZT typically holds a substantial amount of residual stresses post processing causing a reduction in the piezoelectric response. As T_{sub} increases, the thermal contribution to this stress stress is gradually relaxed, which will move the operation point away from the saturation point in the piezoelectric hysteresis. Due to increased linearity, any such stress-relaxation is expected to increase the piezoelectric response which is indeed observed here. Also, the highly nonlinear α of Silicon will in the current temperature range cause the largest thermal stress-relaxation of the stack to occur between 25^oC and 100^oC and may therefore be an additional contribution. Also, it can be mentioned that increased domain wall mobility with temperature will have a positive effect on the unipolar strain [6].

B. *Humidity-related degradation*

Micrographs of the bonding pads after device failure is shown in *Fig. 3* (a). Humidity-related degradation was primarily manifested as local breakdown-events and pinhole-formation along the edges and on top of all utilized top electrodes. The ground pads and unused electrodes, however, remained unaffected. As shown in *Fig. 3* (a), the relative pinhole concentration appeared to be considerably larger along the electrode edges than on top of the electrode surfaces. Also, the total number and relative portion of pinholes along the edges compared to the electrode surface was significantly larger at lower T_{sub} than at higher T_{sub}. Since for the present experiments the applied voltage was above the standard potential for catalytic water-splitting of $1.23\ V$, we speculate that water-splitting catalysis can facilitate the observed degradation. During testing, the Ti/W-layer used as an adhesion-layer between Au and PZT is exposed to the ambient along the electrode edges and can hence form catalytically active oxides such as TiO_2 and WO_3 in the presence of humidity. If water-splitting is indeed occurring, hydrogen will evolve on the top electrode and may quickly diffuse into PZT along the electrode edges. If e.g. hydrogen-induced hardening reduces the critical stress - the maximum stress the PZT-films can accommodate before cracking - so that the application of σ_P results in cracks, the edges should be the first area to be affected by such degradation. The fact that the unused and bottom electrodes remains unaffected may indeed further support this claim and similar observations have been reported for PZT under DC-bias [9], [10] and in the FERAM-literature [11].

For water splitting to occur on the electrode surface, PZT should either be exposed through the top electrode or catalysis should occur on Au. The former can be true in the presence of pinholes, large local defects such as sputtered particles or cracks appearing during operation. The latter have recently caught interest in literature due to the catalytic activity of gold [12]. To understand the connection of the observed degradation to elevated temperatures, the adsorption of water on the device

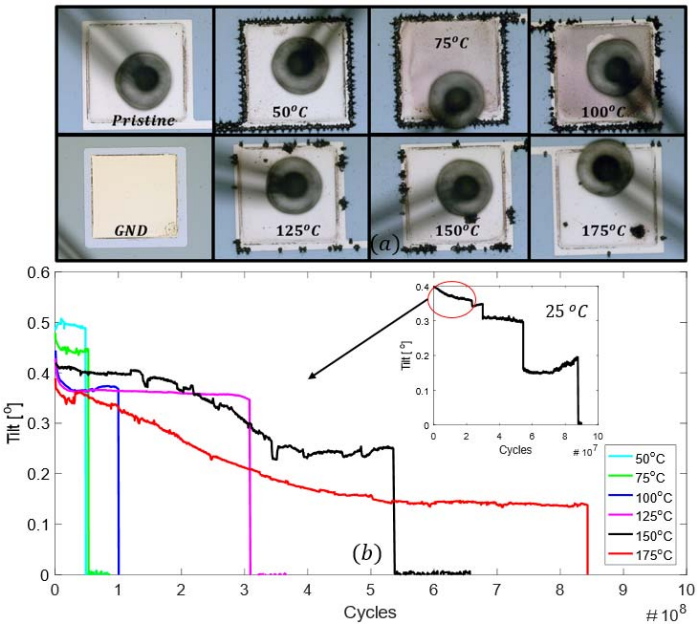

Figure 3: (a): micrographs of bonding pads after failure at $25 - 175^oC$ in humid ambient and (b): measured deflection as a function of cycles.

surface must be discussed. In humid ambient, the surface of perovskite oxides, including PZT, will quickly saturate with a thermally stable layer of chemisorbed hydroxide species and PZT is therefore by itself not severely affected by humidity in the absence of applied voltages, e.g. far away from the used electrodes [13]. Gold on the other hand, is chemically inert and will facilitate molecular adsorption of water [14]. The number of adsorbed molecules depend on the heat of adsorption and desorption of water at a given relative humidity (RH) and T_{atm}. For $RH < 60\%$ the water adsorbed on gold can be approximated by the Brunauer–Emmett–Teller (BET) theory:

$$M_W = \frac{cRH}{(1-RH)(1+RH(c-1))}\ [\frac{\mu g}{cm^2}] \qquad (3)$$

Here M_W is the number of adsorbed monolayers, $c = e^{\frac{Q_i - Q_v}{RT_i}}$ a material-related constant, Q_i and Q_v the heat of water adsorption and desorption, R the universal gas constant and T_i the temperature at the interface between the electrode and the ambient. For gold surfaces up to $T_i = 60\ ^oC$, the net heat of adsorption is small, i.e. $Q_i \approx Q_v$. In this temperature range M_W primarily depends on the relative humidity; $M_W \approx \frac{RH}{1-RH}$ [14]. Since increasing T_{atm} will increase the dew-point and hence reduce the ambient RH as shown in $Fig.\,2\ (c)$, the number of adsorbed monolayers will decrease. It should also be noted that since the device is heated from below, T_i is always larger than T_{atm} and M_W will be even lower at the interface. E.g. as T_{sub} approaches $175\ ^oC$, T_{atm} will approach $62\ ^oC$. Since c will decrease exponentially with T_i, M_W and therefore the degradation rate, will decrease as is presently observed. On the other hand, if the device was heated from above by the ambient the degradation rate would be expected to increase. Below $60\ ^oC$, at higher RH-values the adsorbed water will due to horizontal interactions form a surface film causing the number of adsorbed molecules to depart from that predicted by BET-theory. Also, it can be mentioned that the amount of adsorbed water molecules will be lower if the surface is clean [14].

These literature findings correlate well with the current measured increasing cycles to failure with increasing T_{sub} (see *Fig. 2* (c) and *TABLE I*). This may suggest that other factors such as the absolute humidity ambient humidity rather than the relative ambient humidity, the relation between the device temperature and the ambient temperature as well as the cleanliness of the device being tested are important to consider during lifetime and reliability tests. It can be noted that no local breakdown-events was observed for devices operated in $RH = 35\ \%$ at $T_{sub} = 25\ ^oC$, and $T_{atm} = 25\ ^oC$ for up to $1.5x10^{11}$ cycles. At $T_{sub} = 175\ ^oC, T_{atm} = 62.3\ ^oC$ and $RH = 15.4\ \%$ on the other hand, failure occurred after $9x10^8$ cycles which further support the abovementioned claim.

The measured amplitude degradation in high humidity was typically characterized by four sudden drops during operation, as shown in the inset of *Fig. 3* (b). Each drop was associated with the breach of an electrode routing connecting the wire-bonding pads to the actuating membrane. Hence, device failure was defined as the breach of the first electrode. The tilt relative to the tilt at $25\ ^oC$ as a function cycles until the first routing breach is plotted vs T_{sub} in the main graph of *Fig. 3* (b). As seen, the deflection amplitude declines by cycling for all devices. But, even though the rate of decline was significantly higher at elevated temperatures, as to be expected [5], the lifetime was indeed longer. However, the electromechanical degradation by cycling was found to exceed the expected contribution from pure ferroelectric fatigue. E.g. at $175\ ^oC$ the average decrease in tilt was $65\ \%$ opposed to a $10\ \%$ decrease in P_S after $5x10^8$ cycles (not shown here). ε_r remained approximately constant throughout the experiments. Again, this points towards the in-plane sensitivity to film-substrate stress transfer and other factors of such devices. Lastly it can be mentioned that no short-circuiting was detected prior to the shown routing breaches.

IV. Summary and Conclusions

Unipolar temperature-humidity-cycling tests with a constant absolute humidity of $22\ g/m^3$ and substrate temperatures from 25^oC to $175\ ^oC$ were carried out to assess the lifetime and reliability of PZT-based piezoelectric micromirrors. For all temperatures, humidity related degradation by local breakdown-events was more pronounced and preceded that related to polarization fatigue. Also, the average initial piezoelectric response and number of cycles to device failure were both found to increase with increasing substrate temperatures.

Acknowledgments

The authors wish to thank A. Vogl, P. Wittendorp and J. Gjessing for their excellent scientific and technical support. The present research was kindly supported by the Research Council of Norway under contract number 247781/O30.

References

[1] C.-B. Eom and S. Trolier-McKinstry, "Thin-film piezoelectric MEMS," *MRS Bull.*, vol. 37, no. 11, pp. 1007–1017, 2012.

[2] T. Bakke et al., "A novel ultra-planar, long-stroke and low-voltage piezoelectric micromirror," *J. Micromechanics Microengineering*, vol. 20, p. 064010, 2010.

[3] I. P. Lipscomb et al., "The effect of relative humidity, temperature and electrical field on leakage currents in piezo-ceramic actuators under dc bias," *Sensors Actuators, A Phys.*, vol. 151, no. 2, pp. 179–186, 2009.

[4] H. Nazeer et al., "Residual stress and Young's modulus of pulsed laser deposited PZT thin films: Effect of thin film composition and crystal direction of Si cantilevers," *Microelectron. Eng.*, vol. 161, pp. 56–62, 2016.

[5] D. Damjanovic, "Ferroelectric, dielectric and piezoelectric properties of ferroelectric thin films and ceramics," *Reports Prog. Phys.*, vol. 61, no. 9, pp. 1267–1324, 1998.

[6] Y. A. Genenko et al., "Mechanisms of aging and fatigue in ferroelectrics," *Mater. Sci. Eng. B Solid-State Mater. Adv. Technol.*, vol. 192, no. C, pp. 52–82, 2015.

[7] M. W. Hooker, "Properties of PZT-Based Piezoelectric Ceramics Between -150 and 250 C," *Lockheed Martin Eng. Sci. Co.*, no. September, p. 28, 1998.

[8] V. M. Glazov and A. S. Pashinkin, "The Thermophysical Properties (Heat Capacity and Thermal Expansion) of Single-Crystal Silicon," *High Temp.*, vol. 39, no. 3, pp. 413–419, 2001.

[9] D. Zheng et al., "Multi-breakdown model for explaining the formation and growth of black spots in PZT capacitor under DC bias," *Sensors Actuators, A Phys.*, vol. 241, pp. 197–202, 2016.

[10] D. Zheng et al., "Current leakage and transients in ferroelectric ceramics under high humidity conditions," vol. 158, pp. 106–111, 2010.

[11] C. Huang et al., "Effect of hydrogen on Pb(Zr,Ti)O3-based ferroelectric capacitors," *J Appl Phys*, vol. 98, no. 98, p. 104105, 2005.

[12] G. M. Mullen et al., "The effects of adsorbed water on gold catalysis and surface chemistry," *Top. Catal.*, vol. 56, no. 15–17, pp. 1499–1511, 2013.

[13] J. M. Polfus et al., "Surface defect chemistry of Y-substituted and hydrated BaZrO 3 with subsurface space-charge regions," *J. Mater. Chem. A*, vol. 4, no. 19, pp. 7437–7444, 2016.

[14] S. Sharma and J. Thomas III, "Adsorption of water vapor on thin gold electroplated on copper," *J. Vac. Sci. Technol.*, vol. 825, pp. 3–5, 1977.